Primary cilia safeguard cortical neurons in neonatal mouse forebrain from environmental stress-induced dendritic degeneration

Seiji Ishii[a,b], Toru Sasaki[a], Shahid Mohammad[a], Hye Hwang[a,c], Edwin Tomy[a], Fahad Somaa[a], Nobuyuki Ishibashi[a], Hideyuki Okano[b], Pasko Rakic[d,1], Kazue Hashimoto-Torii[a,d,e,1], and Masaaki Torii[a,d,e,1]

[a]Center for Neuroscience Research, Children's Research Institute, Children's National Hospital, Washington, DC 20010; [b]Department of Physiology, Keio University School of Medicine, Tokyo 160-8582, Japan; [c]Institute of Biomedical Sciences, School of Medicine and Health Sciences, The George Washington University, Washington, DC 20052; [d]Department of Neuroscience, School of Medicine, Yale University, New Haven, CT 06520-8001; and [e]Department of Pediatrics, Pharmacology and Physiology, School of Medicine and Health Sciences, The George Washington University, Washington, DC 20052

Contributed by Pasko Rakic, November 13, 2020 (sent for review June 29, 2020; reviewed by Joseph Gleeson and Dan Goldowitz)

The developing brain is under the risk of exposure to a multitude of environmental stressors. While perinatal exposure to excessive levels of environmental stress is responsible for a wide spectrum of neurological and psychiatric conditions, the developing brain is equipped with intrinsic cell protection, the mechanisms of which remain unknown. Here we show, using neonatal mouse as a model system, that primary cilia, hair-like protrusions from the neuronal cell body, play an essential role in protecting immature neurons from the negative impacts of exposure to environmental stress. More specifically, we found that primary cilia prevent the degeneration of dendritic arbors upon exposure to alcohol and ketamine, two major cell stressors, by activating cilia-localized insulin-like growth factor 1 receptor and downstream Akt signaling. We also found that activation of this pathway inhibits Caspase-3 activation and caspase-mediated cleavage/fragmentation of cytoskeletal proteins in stress-exposed neurons. These results indicate that primary cilia play an integral role in mitigating adverse impacts of environmental stressors such as drugs on perinatal brain development.

cortical neurons | dendrite | environmental stress | ketamine | primary cilia

Exposure to harmful environmental factors during prenatal and perinatal stages of human brain development can disrupt a number of molecular pathways involved in critical steps of brain development, potentially leading to the development of neurodevelopmental disorders or intellectual disabilities (1, 2). Of those factors, alcohol and ketamine represent major drugs that are frequently used by pregnant women (3, 4). These two drugs share γ-minobutyric acid (GABA) mimetic and *N*-methyl-D-aspartic acid (NMDA) antagonistic properties, which have been shown to mediate strong cell death-promoting effects in the developing brain (5, 6). Exposing mice to alcohol or anesthetics, such as ketamine, at about postnatal day (P) 7 is commonly used to model exposure of human fetuses between the third trimester of gestation and the neonatal stage. During this critical period, a brain undergoes a growth spurt (7), and disruption of developmental processes during this period is particularly harmful, often triggering long-term brain dysfunctions.

Alcohol (ethanol) exposure can perturb essential processes in brain development, including neurogenesis, migration, and cell survival (8), leading to a wide range of functional deficits (9–13). Many studies have revealed that immature neurons are particularly vulnerable targets for ethanol-induced apoptotic cell death during the brain growth spurt (14).

Ketamine is used as an analgesic and anesthetic for surgery, and has also emerged as an effective antidepressant (15, 16). However, ketamine is also abused as a recreational drug (17). Increasingly widespread use and misuse of ketamine by pregnant and lactating women, raises concerns about its neurotoxicity to the immature perinatal brain of their offspring (18, 19). In a number of animal and human studies, perinatal exposure to ketamine was shown to trigger neuronal degeneration, which subsequently leads to long-term and permanent functional deficits (20–22).

Under the risk of exposure to such factors, the developing brain relies on various intrinsic neuroprotective mechanisms including heat shock signaling and endoplasmic reticulum stress pathways (23, 24). Increasing attention has been paid to these pathways as attractive targets for the development of novel interventions and therapies for neuropsychiatric and neurodegenerative disorders (24, 25). Yet, our understanding of the intrinsic protective mechanisms remains limited.

Cilia, which consist of motile and primary types, are protuberances that project from the soma of various cell types (26, 27). Primary cilia are known to play a pivotal role in early normal brain development (28) by regulating the signal transduction of key molecular pathways such as Hedgehog and Wnt signaling (29). The elongation (maturation) of primary cilia in the cerebral cortex occurs during early postnatal development in mice (around P0 to P14) (27), and deficits are suspected to be involved in the pathogenesis of neuropsychiatric disorders such as autism and schizophrenia (30–32). Although the risk for these disorders is known to be increased by exposure to various environmental stressors, including alcohol and ketamine (33–35), it is unknown

Significance

External agents, such as alcohol and ketamine, are known to affect perinatal brain development and eventually cause a variety of severe psychopathological consequences. However, the mechanisms of possible neuronal defense against these agents are not well understood. We sought to elucidate the molecular details of the role of primary cilia in this complex process. Our results show that primary cilia protect dendrites of immature cortical neurons via insulin-like growth factor 1 receptor and downstream Akt signaling. These results provide insight into the pathogenesis of consequences that follow exposure to toxic substances.

Author contributions: S.I., K.H.-T., and M.T. designed research; S.I., T.S., S.M., H.H., E.T., F.S., K.H.-T., and M.T. performed research; S.I., T.S., S.M., P.R., K.H.-T., and M.T. analyzed data; and S.I., N.I., H.O., P.R., K.H.-T., and M.T. wrote the paper.

Reviewers: J.G., University of California San Diego; and D.G., University of British Columbia.

Competing interest statement: H.O. is a founding scientist of SanBio Co. Ltd. and K Pharma Inc.

[1]To whom correspondence may be addressed. Email: pasko.rakic@yale.edu, khtorii@childrensnational.org, or MTorii@childrensnational.org.

This article contains supporting information online at https://www.pnas.org/lookup/suppl/doi:10.1073/pnas.2012482118/-/DCSupplemental.

Published December 28, 2020.

whether cilia play a role in preserving normal brain development in the face of environmental factors.

In the present study, we tested whether primary cilia serve a protective role during exposure of the developing cerebral cortex to environmental insults such as ethanol and ketamine. We used transgenic mice in which cilia are genetically lost in cortical excitatory neurons as a model system. Our data provide evidence that primary cilia are an essential organelle for efficient activation of cilia-localized insulin-like growth factor 1 receptor (IGF-1R), and downstream Akt signaling to protect immature neurons from caspase-mediated dendritic degeneration in the developing brain.

Results

Loss of Primary Cilia Augments Environmental Stress-Induced Caspase-3 Activation in the Developing Cerebral Cortex. To determine the roles of cilia in brain development under exposure to environmental insults, we employed conditional knockout (cKO) of intraflagellar transport 88 (*Ift88*), a gene required for cilia formation and maintenance (36). *Ift88* floxed mice were crossed with mice carrying the transgene *Emx1-IRES-Cre* (*Emx1-Cre*) by which Cre recombinase is expressed specifically in the dorsal pallium-originated cortical cells (37). In contrast to conditional heterozygote (cHet) control mice, in which each cortical neuron has one primary cilium at the somal region (27) (Fig. 1*A*), loss of cilia in cortical excitatory neurons (Fig. 1*A*), but not in cortical interneurons (Fig. 1*B*), was confirmed in cKO mice. No obvious structural abnormalities were observed in the brain of cKO mice as previously reported (38, 39).

Ethanol (EtOH) was administered by subcutaneous (s.c.). injection on P7 at 2.5 g/kg weight twice with a 2-h interval (Fig. 1*C*). Using this regimen, activation of Caspase-3, a key effector in the process of apoptotic cell death, was observed in the soma of cortical pyramidal neurons in layers II and V in cHet animals as early as 4 h post (second) injection (*SI Appendix*, Fig. S1*A*), similar to cases of EtOH-exposed wild-type mice (40–42). Strikingly, in *Ift88* cKO mice, the activation of Caspase-3 was highly augmented in the soma as well as the main stem of apical dendrites (*SI Appendix*, Fig. S1*A*). The number of activated Caspase-3-positive neurons remained small 24 h postinjection in cHet mice, while the number was significantly larger in cKO mice, particularly in layer V (Fig. 1 *D–F*). By then, labeling of activated Caspase-3 became widely scattered, likely in dendritic arbors, in EtOH-exposed cKO mice (Fig. 1*D*). The expression of activated Caspase-3 was no longer detectable 72 h postinjection (*SI Appendix*, Fig. S1*B*). No obvious activation of Caspase-3 was observed at any time point following phoshate-buffered saline (PBS; control) exposure in either cHet or cKO mice (Fig. 1 *D–F* and *SI Appendix*, Fig. S1).

Ketamine administration (by a single s.c. injection on P7 at 20 mg/kg weight) yielded similar results. Compared with little to no activation of Caspase-3 in the cortex of both cHet and cKO mice in the control (PBS) condition, a small number of Caspase-3-positive cells were observed in layers II and V in ketamine-exposed cHet mice 24 h postinjection, and the number was drastically increased in cKO mice (Fig. 1 *G–I*). These results suggest that primary cilia promote neuroprotection in the immature brain exposed to these environmental factors.

Loss of Primary Cilia Causes Defects in Dendritic Arbors in the Cerebral Cortex Exposed to Environmental Stress. To characterize the potential neuroprotective roles of cilia across multiple neuronal subpopulations, we quantified the number of neurons from cortical layer V, where robust EtOH-induced Caspase-3 expression was found, for each of several distinct neuronal subtypes at P21 (Fig. 2*A*). Surprisingly, across each neuronal subtype examined (i.e., neurons expressing COUP-TF interacting protein 2 [Ctip2], mu-crystallin [Crym], or Thymocyte differentiation antigen 1 fused with yellow fluorescent protein [Thy1-YFP]), the number of neurons counted was not significantly different among the four treatment groups (cHet or cKO mice exposed to PBS or EtOH) (Fig. 2*B* and *SI Appendix*, Fig. S2). Instead, we found a reduction in dendritic complexity; Thy1-YFP-labeled layer V neurons in EtOH-exposed cKO mice exhibited fewer dendrites with fewer and shorter branches than those in other groups (Fig. 2 *C–F*). On the other hand, dendritic spines were found in normal number and morphology on apical and basal dendrites in EtOH-exposed cKO mice (*SI Appendix*, Fig. S3).

These findings corroborate recent reports that caspases contribute not only to cell death but also to various physiological and pathological nonapoptotic events, including axon and dendritic pruning and degeneration, through cleavage of distinct protein targets (43). Indeed, we found a significant increase in caspase-mediated fragmentation/cleavage of β-actin and α-tubulin cytoskeletal proteins, which are hallmarks of developmental and pathological neurite degeneration (44–46) in layers II and V in EtOH-exposed cKO mice 24 h postinjection (Fig. 2 *G–K*).

A rapid microglial response, which includes extension and reorientation of microglial processes toward degenerating neuronal processes, has also been reported to occur during the acute phase of dendritic degeneration (47, 48). In our study, we observed that the number of Iba1-positive microglia in layers II and V in cKO mice increased significantly compared with that of the other three groups 24 h post EtOH injection (*SI Appendix*, Fig. S4 *A* and *B*), at which point the activation of Caspase-3 had been observed (Fig. 1*D*). We also found that microglia exhibited larger cell bodies and longer branches with more complex morphology than those in cHet mice exposed to EtOH (*SI Appendix*, Fig. S4 *A* and *C–E*), indicating dynamic microglia activity in response to dendritic degeneration. Given that microglia lack both primary cilia (49) and *Emx1-Cre* expression, it is unlikely that a microglial response is responsible for the degenerative phenotype observed in neurons of the cKO mice. These results collectively indicate a role of primary cilia to suppress stress-induced caspase activation, and protect cortical neurons from caspase-mediated degeneration of dendritic arbors.

Cilia Mediate Cell-Autonomous and Non-Cell-Autonomous Neuroprotection. In our cKO mouse model, primary cilia are lost in the *Emx1-Cre* lineage, which includes most cortical cells, including excitatory neurons and glia (astrocytes and oligodendrocytes) originated from the dorsal pallium (37). To gain insight into cell-autonomous and non-cell-autonomous impacts of cilia loss, we limited cilia loss to a subset of layer V neurons by crossing floxed *Ift88* mice with *ER81-CreERT2;Ai9* transgenic mice (Fig. 3*A*). Following tamoxifen administration, we found robust tdTomato expression at P8 in layer V neurons, and confirmed the loss of primary cilia in *Ift88* conditional homozygous knockout mice (Fig. 3*B*). In these mice, augmented Caspase-3 activation, as compared to that seen in *Ift88* heterozygous knockout mice, was observed in layer V 24 h post EtOH injection (Fig. 3*C*), indicating that primary cilia within the population of layer V neurons contribute to neuroprotection, although this does not exclude the possibility that glial primary cilia may also contribute to neuroprotection. In these mice, the prevalence of activated Caspase-3 puncta was significantly increased in tdTomato-positive neurons (Fig. 3 *C–E*), while we also observed augmented Caspase-3 activation in tdTomato-negative cells surrounding tdTomato-positive neurons (Fig. 3*D*), suggesting that cilia confer neuroprotective properties in both cell-autonomous and non-cell-autonomous manners.

Primary Cilia Are Required for Efficient Activation of Cilia-Localized IGF-1R and Downstream Akt Signaling to Protect Neurons from Environmental Stress. Insulin-like growth factor 1 (IGF1) promotes neuroprotection by triggering autophosphorylation of its receptor, IGF-1R, and initiating the PI3 kinase/Akt (also known

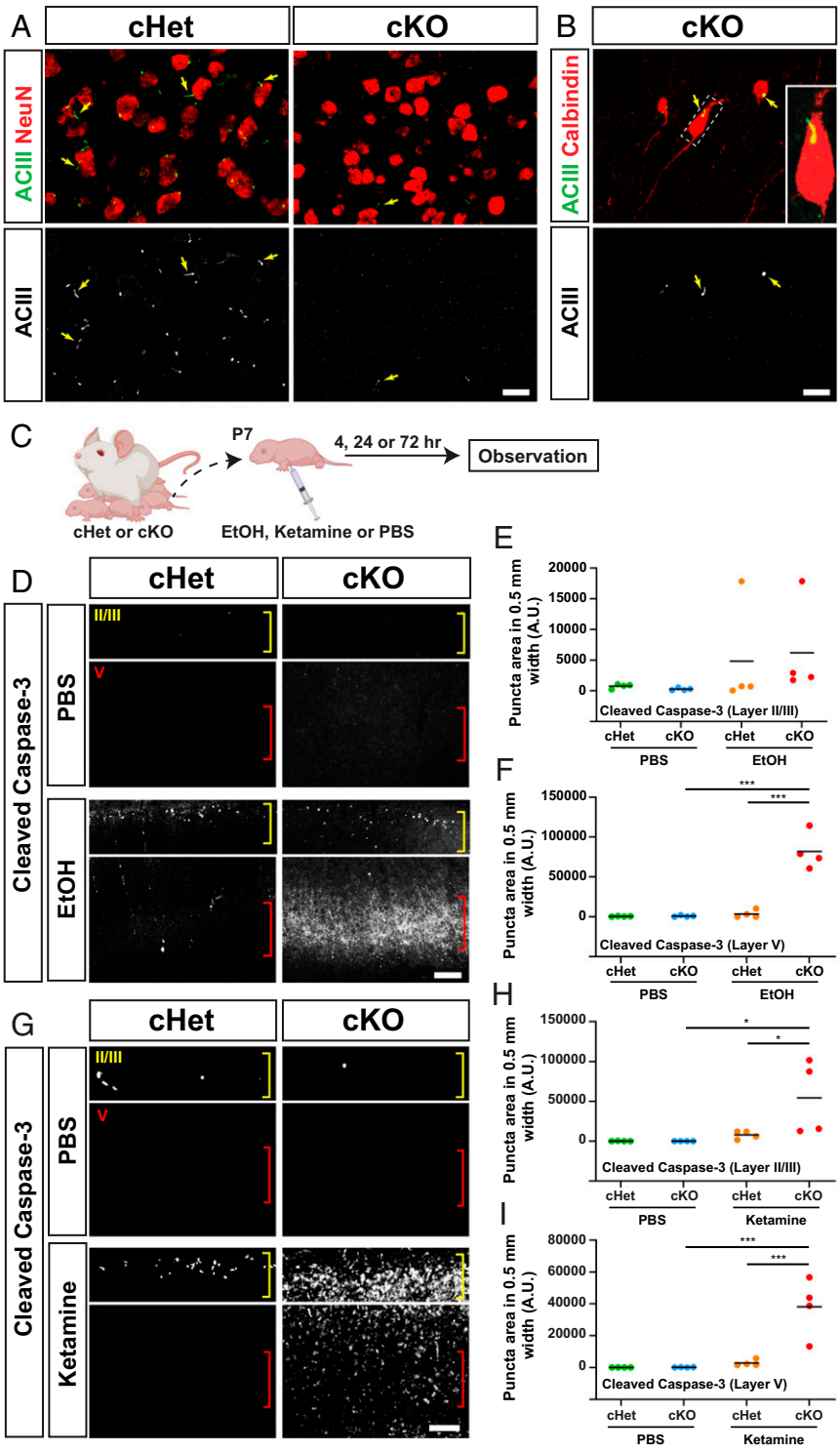

Fig. 1. Caspase-3 activation by exposure to environmental stress is augmented in the cortex of *Ift88* conditional knockout mice. (*A*) Adenylyl cyclase type 3 (ACIII)-labeled (green or white) ciliary axonemes, found in each NeuN-positive (red) cortical neuron within the primary motor cortex (M1) in cHet mice, is absent from excitatory neurons in cKO mice at P90. (Scale bar, 20 μm.) (*B*) Axonemes (arrows) are observed in calbindin-positive interneurons in the cKO cortex. *Inset* shows a higher magnification view of boxed area. (Scale bar, 20 μm.) (*C*) Experimental scheme. (*D*) Immunohistochemistry for cleaved Caspase-3 in M1 24 h after exposure to EtOH, showing increased levels of activated Caspase-3 in layers II and V in cHet mice and further augmentation in cKO mice, particularly in layer V. Layers II/III and V are indicated with yellow and red brackets, respectively. (Scale bar, 200 μm.) (*E* and *F*) Quantification of cleaved Caspase-3 puncta in layers II (*E*) and V (*F*) (counted in a 500-μm width in M1). The line indicates the mean. ***$P < 0.001$ by simple main effect test following two-way ANOVA. (*G*) Immunohistochemistry for cleaved Caspase-3 in M1 24 h after exposure to ketamine, showing the increase of activated Caspase-3 in cHet mice and further augmentation in cKO mice. (Scale bar, 200 μm.) (*H* and *I*) Quantification of cleaved Caspase-3 puncta in layer II (*H*) and V (*I*). The line indicates the mean. *$P < 0.05$, ***$P < 0.001$ by post hoc Tukey or simple main effect test following two-way ANOVA.

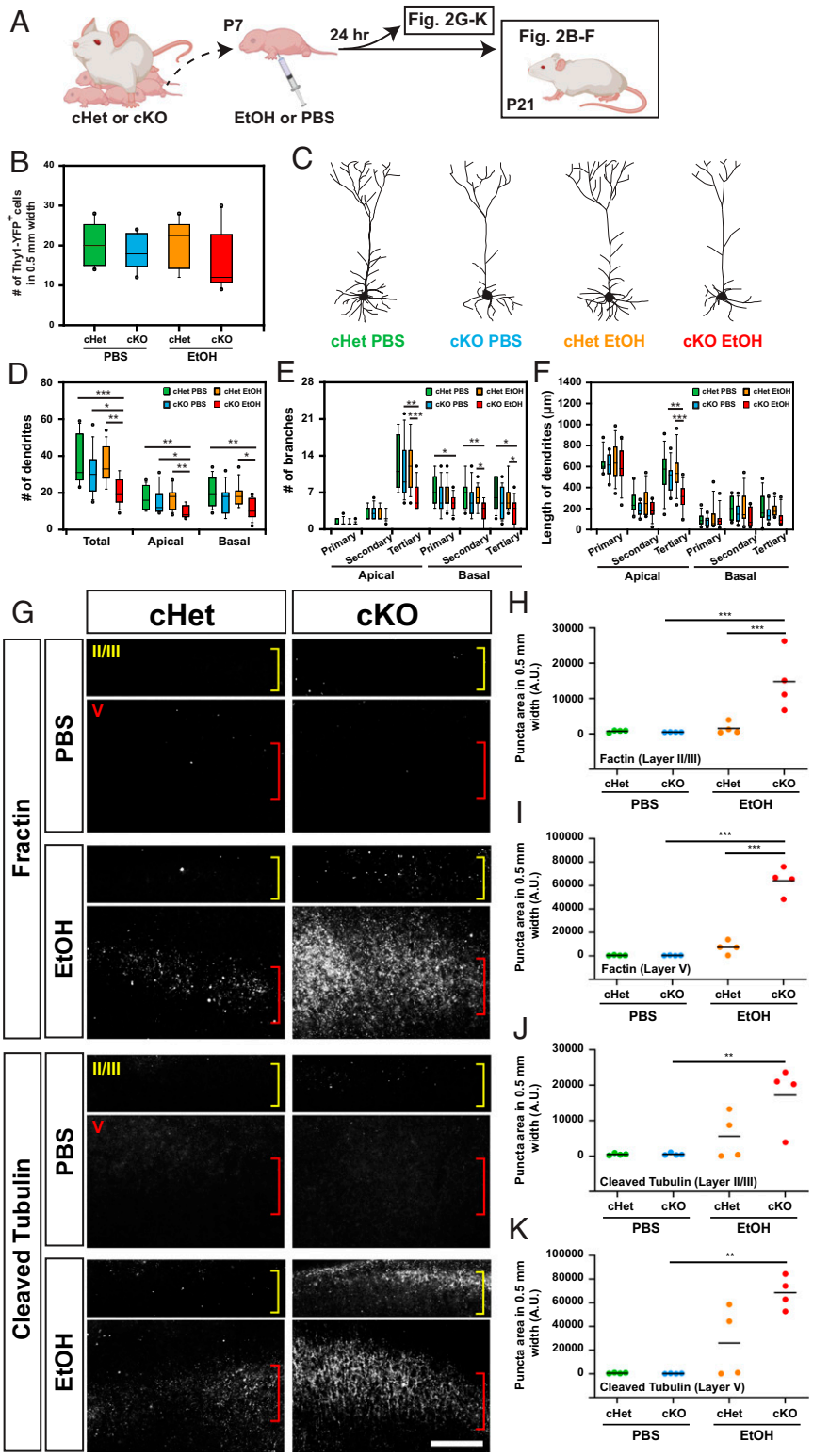

Fig. 2. Caspase-mediated degeneration of dendritic arbors in the EtOH-exposed cortex is augmented in cKO mice. (*A*) Experimental scheme. (*B*) The number of Thy1-YFP-positive neurons per cortical column of 500-μm width in M1, showing no significant differences between the four groups at P21. (*C*) Representative morphologies of Thy-1 YFP-positive neurons in the indicated conditions. (*D–F*) Quantification of the number of dendrites (*D*) and branches per neuron (*E*), and the length of dendrites (*F*), showing significant reduction in dendritic complexity of neurons in EtOH-exposed cKO mice compared with those in other groups. The line indicates the mean. $*P < 0.05$, $**P < 0.01$, $***P < 0.001$ by post hoc Tukey or simple main effect test following two-way ANOVA. (*G*) Immunohistochemistry for caspase-cleaved actin (fractin) and caspase-cleaved tubulin in M1, showing their increase in layers II and V in cHet mice 24 h after exposure to EtOH, with further augmentation in cKO mice. Layers II/III and V are indicated with yellow and red brackets, respectively. (Scale bar, 200 μm.) (*H–K*) Quantification of fractin (*H* and *I*) or cleaved tubulin (*J* and *K*) puncta in layer II (*H* and *J*) and V (*I* and *K*). The line indicates the mean. $**P < 0.01$, $***P < 0.001$ by post hoc Tukey or simple main effect test following two-way ANOVA.

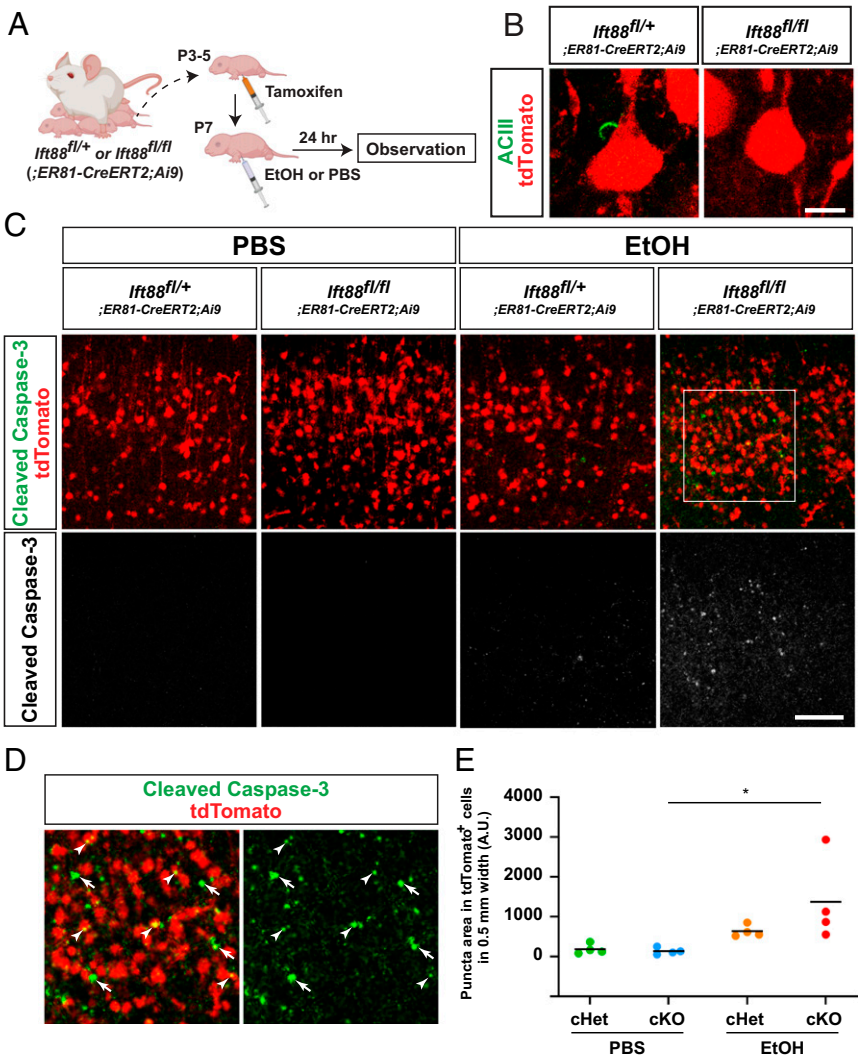

Fig. 3. Neuronal cilia suppress Caspase-3 activation in EtOH-exposed cerebral cortex. (*A*) Experimental scheme. (*B*) tdTomato-labeled layer V neurons have ciliary axonemes (green) in ER81-lineage neuron-specific *Ift88* conditional heterozygous mice but not in conditional homozygous knockout mice. (Scale bar, 10 μm.) (*C*) Activated Caspase-3 (green or white) within tdTomato-labeled (red) cortical layer V in M1 in the indicated genotype × treatment groups 24 h postexposure, showing augmented Caspase-3 activation in EtOH-exposed conditional homozygous knockout mice. (Scale bar, 100 μm.) (*D*) Higher magnification view of boxed area in *C*, showing augmented caspase activation in tdTomato-positive neurons (arrowheads) as well as in tdTomato-negative surrounding cells (arrows). (*E*) Quantification of activated Caspase-3 puncta within TdTomato-positive neurons in layer V in M1. $*P < 0.05$ by post hoc Tukey test following two-way ANOVA.

as Protein kinase B) signaling cascade (50). IGF-1R expression is abundant in the embryonic and postnatal brain, but declines during adolescence and adult life (51). Importantly, IGF-1Rs located in primary cilia have been shown to be more sensitive to ligand stimulation than those not located in cilia (52). We, therefore, explored the possibility that primary cilia are required for efficient and acute activation of IGF-1R signaling to protect immature neurons during exposure to environmental insults. To test this possibility, activation of IGF-1R signaling was first assessed in the brain of (*Emx1-Cre*-driven) cHet and cKO mice 24 h after exposure to EtOH at P7. Activation of IGF-1R was clearly detectable by immunohistochemistry for phosphorylated IGF-1R (pIGF-1R) in EtOH-exposed cHet mice (Fig. 4 *A* and *C*). Labeling was primarily found next to the base of cilium labeled by immunohistochemistry for pericentrin (Fig. 4*B*), likely at the ciliary transition zone between the ciliary axoneme and basal body as previously shown in neural progenitor cells (53). In contrast, pIGF-1R was undetectable in EtOH-exposed cKO mice (Fig. 4 *A* and *C*), indicating that primary cilia play a critical role in transducing high-level IGF1 signaling in response to EtOH exposure. Exposure to PBS did not induce detectable levels of IGF-1R activation in cHet or cKO mice (Fig. 4 *A* and *C*).

Next, to examine the contribution of downstream Akt signaling to neuroprotection from environmental stress, we administered a specific activator of cytosolic Akt, small molecule SC79 (54), 30 min before the first EtOH injection in cKO mice at P7, and again 6 h later to force the activation of Akt (Fig. 4*D*). In these cKO mice, Caspase-3 activation in layer II and V neurons 24 h after exposure was significantly reduced compared to the strong activation observed in cKO mice that received control (vehicle only) administration (Fig. 4 *E*–*G*). Consistent with this, dendritic atrophy in EtOH-exposed cKO mice, as observed at P21, was prevented by daily injections of SC79 from P7 to P9 (Fig. 4 *H*–*L*). SC79 administration had no significant effects in PBS-exposed animals (Fig. 4 *H*–*L*). These results demonstrate that cilia-localized IGF-1R and downstream Akt signaling are necessary for the neuroprotective function of cilia in cortical neurons.

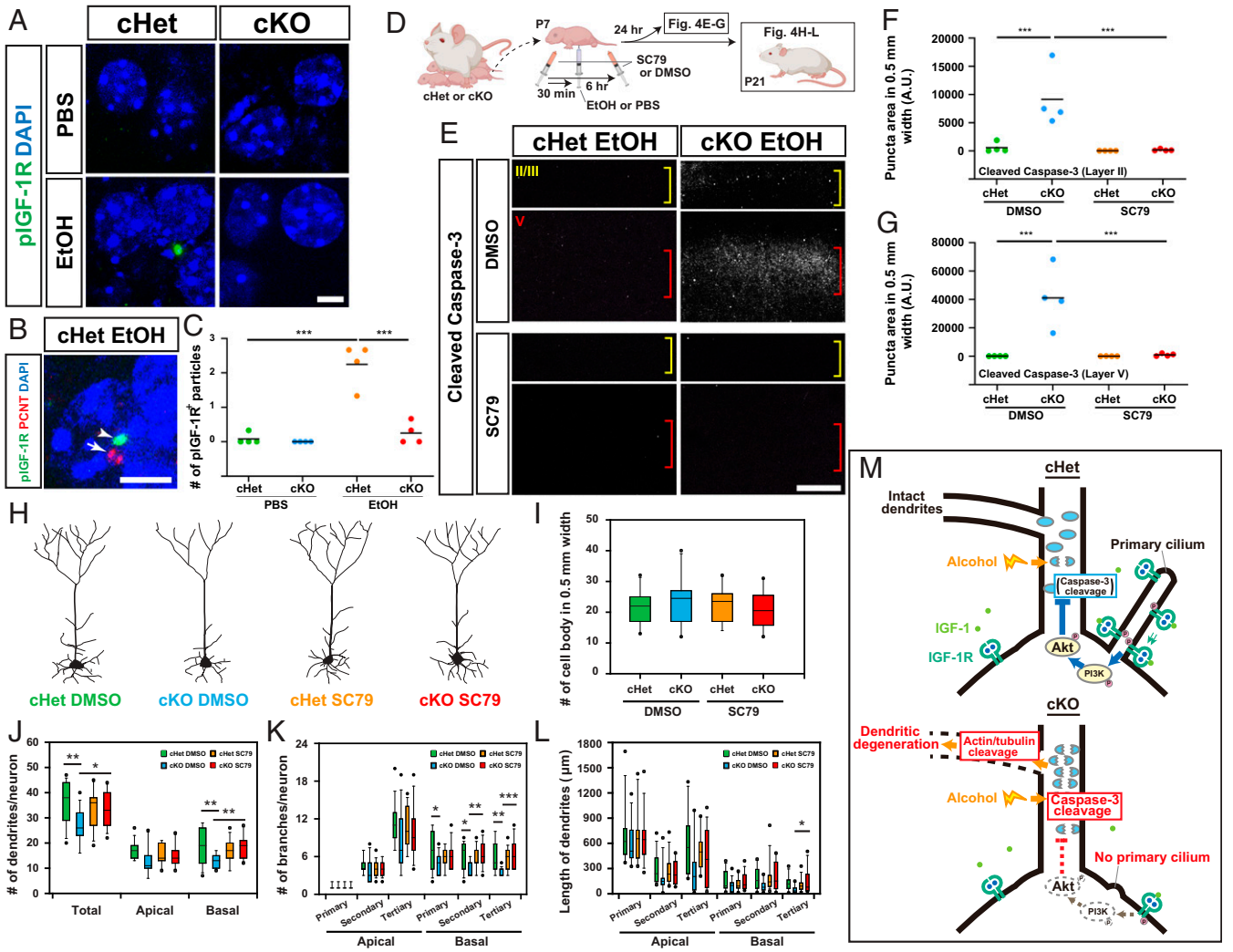

Fig. 4. Activation of ciliary IGF-1R and downstream Akt signaling mediates neuroprotection from EtOH exposure. (*A*) Immunohistochemistry for phospho-IGF-1R (pIGF-1R, green) in layer V neurons in M1 in the indicated conditions 24 h postexposure (see Fig. 1*C* for scheme). Cells are nuclear counterstained with DAPI (blue). (Scale bar, 5 μm.) (*B*) Double staining for pIGF-1R (green) and pericentrin (PCNT, red), showing the accumulation of pIGF-1R (arrowhead) in the region adjacent to the PCNT-labeled ciliary base (arrow). (Scale bar, 5 μm.) (*C*) Quantification of pIGF-1R particles per 8,000 μm^2 in cortical layer V, showing significant increase in cHet mice exposed to EtOH compared with those in other groups. The line indicates the mean. ***$P < 0.001$ by simple main effect test following two-way ANOVA. (*D*) Experimental scheme for treatment with SC79. (*E–G*) Immunohistochemistry for cleaved Caspase-3 in M1 (*E*) and quantification of cleaved Caspase-3 puncta (counted in 500 μm width in M1) in layers II (*F*) and V (*G*) in EtOH-exposed cHet and cKO mice administered with SC79 or DMSO (control). The increase in cleaved Caspase-3 puncta by exposure to EtOH in cKO mice is mitigated by SC79 administration in both layers. Yellow and red brackets in *E* indicate layers II/III and V, respectively. The lines in *F* and *G* indicate the mean. ***$P < 0.001$ by simple main effect test following two-way ANOVA. (Scale bar, 200 μm.) (*H*) Representative morphologies of Thy1-YFP-positive neurons in the indicated conditions. (*I*) No differences were found in the number of Thy1-YFP-positive neurons (in 500-μm width in M1) between the four groups at P21. The line indicates the mean. (*J–L*) Quantification of primary/secondary/tertiary dendrites (*J*) and branches per neuron (*K*), and the length of dendrites (*L*) in Thy1-YFP-positive pyramidal neurons, showing that SC79 administration mitigates the reduced complexity of dendritic morphology in EtOH-exposed cKO mice. The line indicates the mean. *$P < 0.05$, **$P < 0.01$, ***$P < 0.001$ by simple main effect test following two-way ANOVA. (*M*) Proposed mechanism of primary cilia-mediated protection of neurons from dendritic degeneration caused by exposure to environmental stress (details in *Discussion*).

Discussion

Our results provide evidence for the role of primary cilia in relaying molecular signals which protect cortical neurons from environmental stress. Fig. 4*M* depicts our model based on our data: 1) Upon exposure to environmental stress such as alcohol, cilia-localized IGF-1R is activated in cortical neurons; 2) activated IGF-1R (and other pathways) leads to intracellular signal transduction via Akt phosphorylation; 3) activated (phosphorylated) Akt directly or indirectly (55, 56) suppresses the activation of Caspase-3, which otherwise would be induced by exposure to environmental stress; and 4) suppression of Caspase-3 activation prevents caspase-mediated cytoskeletal degradation and ensuing degeneration of dendrites.

In contrast to our results indicating that dendritic growth is normal in the absence of environmental stress among cortical neurons lacking primary cilia (*Ift88* cKO) (Fig. 2), a previous study found that the loss of cilia via dominant negative Kif3a expression resulted in impaired dendritic outgrowth in primary cultured cortical neurons (57). This difference may be explained by differential effects of *Kif3a* and *Ift88* ablations on microtubules projecting from the basal body of the cilium (58, 59) and/or differences between in vitro culture conditions and in vivo environments (e.g., potentially higher oxidative stress in cell cultures) (60). Our results, however, do not exclude the possibility that impaired dendritic growth/arborization may also occur in

parallel to dendritic degeneration in cKO mice exposed to environmental stress.

Of note, neurons in layers II and V were most severely affected in cKO mice exposed to environmental stress at P7. These neurons may require the neuroprotective support provided by cilia more so than other cell types during this vulnerable period, in which long axonal projections branch extensively at their target regions (61). A recent study has shown that layer V neurons (and layer II neurons to some extent) require microglia-derived IGF1 for their survival throughout normal development in earlier stages (P3 to P5) in mice (62). Regardless of stress exposure, we didn't observe a loss of layer V neurons from the cortex of cKO mice at P7 (Fig. 2 and *SI Appendix*, Fig. S2), despite these neurons lacking cilia. Activation of IGF-1R that is not localized to cilia may therefore provide sufficient levels of IGF1 signaling for neuronal survival at this stage.

Although we did not observe cell death, we found a robust increase in Caspase-3 activation in cortical neurons from cKO mice exposed to EtOH or ketamine. The neurotoxicity of GABA mimetics and NMDA antagonists in the developing brain has been extensively studied in various animal models. By immunohistochemistry, Olney and colleagues have shown very robust activation of Caspase-3 even in the brain of wild-type mice by exposure to EtOH at P7 (40, 63). In contrast, with the same treatment condition, we observed weaker Caspase-3 activation by EtOH in our control (cHet) animals. A likely reason for this difference would be because Olney and colleagues observed the brain at 8 h post EtOH exposure, while we did at 4, 24, and 72 h after exposure to compare between cKO and cHet mice. In fact, the quantitative analysis by Olney and colleagues using Western blotting has indicated that the level of activated Caspase-3 changes over time; it becomes detectable at 8 h, peaks at 12 h, and decreases to an undetectable level at 24 h after EtOH exposure (40). Although the activation of Caspase-3 has been used as a marker for apoptotic cell death in many of these previous studies (40, 63–65), more recent studies have found that caspase activation is also involved in various nonapoptotic processes such as immunity and cell fate determination, depending on the degree of activation, intracellular domain, and substrate specificity (43, 66, 67). Our results provide support for nonapoptotic roles of caspase activation, specifically its role in neurite degeneration that occurs independently of cell death, via cleavage of actin and tubulin cytoskeletal molecules (43–45, 68–70). Punctate distribution of fractin and cleaved tubulin in layers II/III and V in EtOH-exposed cKO brains (Fig. 2) is consistent with previous reports showing the punctate labeling in degenerating axons and dendrites (45, 46), and is likely correlated with the distribution of activated Caspase-3 that also shows a punctate pattern (Fig. 1). As the effect of a pan-caspase inhibitor to suppress EtOH-induced cleavage of Caspase-3 in the P7 brain has been shown (71), our results suggest that caspase inhibitors have therapeutic potential to prevent dendritic degeneration by perinatal EtOH exposure. The level of activated Caspase-3, fractin, and cleaved tubulin in the brain of EtOH-exposed cKO mice exhibited large variability across individual animals (Figs. 1–4). Such variability may be primarily introduced by the complexity of gene–environment interactions, although we do not exclude possible involvement of other factors such as variations in the genome sequence reported even within an inbred strain (72–74).

We found that IGF-1R was activated at the ciliary transition zone upon exposure to EtOH using immunofluorescence staining (Fig. 4*B*), although the exact mechanisms responsible for receptor activation require further investigation. This staining was absent in cKO mice. A previous study has shown that loss of cilia in preadipocytes by Ift88 knockdown causes overall decrease of pIGF-1R (52). This study also has shown that loss of cilia causes a marked decrease in IGF-1R signaling-mediated Akt-1 activation not only at the transition zone but also throughout the cell. Therefore, although we were able to detect only the most obvious decrease at the transition zone, EtOH-induced pIGF-1R may be similarly decreased throughout the cell by the loss of cilia. Activation of IGF-1R by EtOH exposure contrasts with previous studies that have reported attenuation of IGF-1R signaling pathways in the developing brain due to chronic EtOH exposure (75, 76). The difference may be due to pleiotropic effects of EtOH depending on cellular context or treatment regimen (77, 78). In fact, it has been shown that EtOH positively and negatively affects Akt phosphorylation at low and high doses, respectively, in hepatic insulin signaling in rats (77). Differential effects on IGF-1R activation based on the type of EtOH treatment (i.e., chronic exposure versus acute low-dose exposure) have also been reported in cultured neurons (79). Cilia-dependent IGF-1R signaling is required for cell-cycle progression in cortical progenitor cells (53, 80) and the differentiation of preadipocytes (52). In both processes, similar to what we observed in stress-exposed cortical neurons, phosphorylated IGF-1Rs are shuttled from the primary cilium toward the ciliary base upon ligand stimulation, allowing for efficient activation of downstream signaling molecules including Akt (53, 81). Thus, cilia-mediated signaling may be prioritized for cellular activities that require immediate and/or efficient IGF-1R signal transduction.

Primary cilia likely mediate other external signals for neuroprotection against environmental stress. For example, Hedgehog (Hh), Wnt, and platelet-derived growth factor (PDGF) signaling pathways, which are also mediated by the primary cilium, have been shown to exert neuroprotective function (82–84). Defects in ciliary signaling may therefore render neurons susceptible to various types of environmental stress. It is also highly likely that cilia play protective roles in cell types other than neurons. For example, an in vitro study has shown that activation of Hh signaling in primary cilia is involved in the survival of astrocytes under starvation (85). In our results, we observed that the loss of cilia in layer V neurons augmented Caspase-3 activation, not only in layer V neurons, but also in cells surrounding these neurons (Fig. 3). This non-cell-autonomous effect may represent an indirect consequence of disrupted intercellular interactions arising due to dendritic degeneration of primarily affected neurons or from altered expression of secreted molecules from these neurons due to deficient cilia-mediated signaling (86). Alternatively, impaired release of ciliary vesicles (87–89) might also be involved in producing non-cell-autonomous effects.

Collectively, our findings indicate that primary cilia play more diverse roles than previously assumed in brain development, a critical biological process which proceeds under the risk of exposure to a variety of environmental factors. Our results suggest that ciliopathy patients may have increased risk of abnormal brain development upon exposure to environmental insults, and this may also underlie the variability in their disease manifestations (90). More subtle alterations in primary cilia due to genetic conditions, in combination with environmental factors, may lead to various neurodevelopmental disorders (32, 91). Therefore, despite the benefits of several factors, such as ketamine as an efficient anesthetic and antidepressant agent, our results urge clinicians and patients with potential deficits in primary cilia to take extra precautions to avoid the risks for long-term negative impacts of those factors. Further studies to define the whole picture of cilia-mediated neuroprotection will help us to advance our understanding of its importance in the pathogenesis of neurodevelopmental disorders.

Materials and Methods

Animals. The animal protocol was approved by the Institutional Animal Care and Use Committee at Children's National Hospital. All methods were performed in accordance with relevant guidelines and regulations. *Ift88*^{fl} (B6.129P2-*Ift88*^{tm1Bky}/J), *Emx1-IRES-Cre* [B6.129S2-*Emx1*$^{tm1(cre)Krj}$/J], *ER81-CreERT2* [B6(Cg)-*Etv1*$^{tm1.1(cre/ERT2)Zjh}$/J], *Ai9* [B6.Cg-*Gt(ROSA)26Sor*$^{tm9(CAG-tdTomato)Hze}$/J], and *Thy1-YFP-H Tg* [B6.Cg-Tg(Thy1-YFP)HJrs/J] mice were obtained from The

Jackson Laboratory (stock nos.: 022409, 005628, 013048, 007909, and 003782, respectively). For conditional deprivation of primary cilia, *Ift88*$^{fl/fl}$ mice were crossed with *Emx1-IRES-Cre* or *ER81-CreERT2;Ai9* mice. Heterozygous knockout mice from the same litter were used as controls. Using 120 single nucleotide polymorphisms across 19 chromosomes, we confirmed that the percent contribution of C57BL/6 to overall genetic background of *Ift88*$^{fl/fl}$ mice was over 90%. All mice were genotyped by Transnetyx.

Drug Administration. cHet and cKO pups were weighed and subcutaneously injected twice with 2.5 g/kg of EtOH (or PBS control) at 2-h intervals or once with 20 mg/kg ketamine (or PBS control) at postnatal day (P) 7. For conditional *Ift88* deletion in *ER81-CreERT2;Ai9* mice, tamoxifen dissolved in corn oil (75 mg/kg) was administrated daily from P3 to P5. Akt Activator II, SC79 (Calbiochem, 123871) was dissolved in dimethyl sulfoxide (DMSO) at 50 mg/mL for stock solution. P7 pups were injected subcutaneously with SC79 (diluted in saline from the stock solution, 40 μg/g weight) or vehicle control (DMSO diluted in saline) 30 min before the first EtOH injection, and again 6 h after the first SC79 injection. For the analysis of dendritic morphology at P21, SC79 (or DMSO control) was injected additionally at P8 and P9.

Immunohistochemistry. Immunohistochemistry was performed as previously described (92, 93). Brains were fixed in 4% paraformaldehyde (PFA) in PBS overnight at 4 °C, and cut into 70 μm-thick coronal sections. The staining was amplified using the TSA Plus system (Perkin-Elmer) or VECTASTAIN ABC system (Vector Laboratories). Monoclonal anti-Calbindin-D-28K (clone CB-955, 1:3,000, Sigma-Aldrich, C9848), anti-NeuN (clone A60, 1:1,000, EMD Millipore, MAB377), anti-cleaved Caspase-3 (Asp175) (clone 5A1E, 1:300, Cell Signaling, 9654), anti-mu Crystallin (Crym) (1:500, Abcam, ab54669), anti-RFP/tdTomato (1:200, Abcam, ab65856), anti-Ctip2 (clone 24B6, 1:500, Abcam, ab18465), anti-IGF1 Receptor α (clone G-5, 1:100, SCBT, sc-271606), and anti-pericentrin (1:200, BD Biosciences, 611815) antibodies were used. Polyclonal anti-adenylate cyclase III (1:10,000, EnCor Biotechnology Inc., RPCA-ACIII), anti-cleaved Caspase-3 (Asp175) (1:400, Cell Signaling, 9661), anti-fractin (1:1,000, EMD Millipore, AB3150), anti-tubulin cleaved by caspase (1:3,000, MediMabs, MM-0143), anti-Iba1 (1:1,000, WAKO, 019-19741), and anti-IGF1 Receptor (phospho Y1161) (1:100, Abcam, ab39398) antibodies were also used. Both monoclonal and polyclonal antibodies for cleaved Caspase-3 provided the same results, and the images obtained using the monoclonal antibody are shown in the figures. Nuclei were counterstained with 4,6-diamidino-2-phenylindole (DAPI) (Sigma-Aldrich). Images were acquired using a Zeiss LSM 510 or Olympus FV1200 confocal microscope or the ApoTome system.

Quantification of Cleaved Caspase-3, Fractin, and Caspase-Cleaved Tubulin Puncta. For the quantification of cleaved Caspase-3, fractin, or caspase-cleaved tubulin puncta in primary motor cortex (M1), images were taken in coronal sections using a 10× objective lens on the Zeiss ApoTome system. Three regions in M1 (500-μm width each) were randomly selected in each brain, and the areas occupied by puncta (arbitrary unit) were measured using ImageJ. For the quantification of cleaved Caspase-3 puncta in tdTomato-positive neurons, the area occupied by puncta within TdTomato-positive neurons in layer V in M1 was measured similarly. Four different brains per group were used for each quantification.

Analyses on the Number and Morphology of Microglia and Pyramidal Neurons. Iba1-positive microglia and Ctip- and Crym-positive neurons in layer V in M1 were imaged in coronal sections at 63× by Olympus FV1200. The number of cells per 2 mm^2, cell body size, number of branches per microglia, and total length of branches per microglia was quantified based on previous methods (94–96).

Morphological Analysis of Dendritic Spines. Spines on apical and basal dendrites of Thy1-YFP-labeled layer V pyramidal neurons in M1 were imaged in coronal sections using a 63× objective with 3× digital zoom using the Olympus FV1200 system and LSM 510 system. Spine density was defined as the number of spines per micrometer by counting the number of spines on dendritic branches of ∼20- to 30-μm length from three neurons per group.

Statistics. Data were subjected to statistical analyses with Prism 7 and 8 (GraphPad). In dot plots, each filled circle represents the average value quantified at each of the three randomly selected regions in M1 in each brain (see also *Quantification of Cleaved Caspase-3*, *Fractin*, *and Caspase-Cleaved Tubulin Puncta* above). For each condition, we collected data from four animals. The horizontal line indicates the mean of the data. In box plots, the bar within the box indicates the median, and the upper and lower edges of the box represent the 25th and 75th percentiles, respectively. The upper and lower whisker boundaries indicate the 10th and 90th percentiles, respectively. All statistical analyses were performed using two-way ANOVA (*F* and *P* values are shown in *SI Appendix*, Table S1) followed by post hoc multiple comparisons. Tukey and simple main effect tests were used as the post hoc test if interactions between variables were insignificant or significant, respectively. A *P* value of less than 0.05 was considered significant.

Data Availability. All study data are included in the article and *SI Appendix*.

ACKNOWLEDGMENTS. We thank Hiroki Naito, Aiesha Basha, and Akihiko Nakata for their technical assistance and Stephen Page for critical reading of the manuscript. This study was supported by NIH/National Institute on Alcohol Abuse and Alcoholism/National Institute of Mental Health/National Heart, Lung, and Blood Institute/National Institute on Drug Abuse R01AA025215 (K.H.-T.), R01MH111674 (M.T.), R21AA024882, R01AA026272 (K.H.-T. and M.T.), R01HL139712, R01HL146670 (N.I.), and R01DA023999 (P.R.); the Scott-Gentle Foundation (K.H.-T. and M.T.); JSPS KAKENHI (Grant-in-Aid for Research Activity start-up; 17H06563, Grant-in-Aid for Scientific Research [C]; 19K07829) (S.I.); a grant-in-aid from Keio University Sakaguchi-Memorial Medical Science Fund (S.I.); the Kawano Masanori Memorial Public Interest Incorporated Foundation for Promotion of Pediatrics (S.I.); and internal budgets from Keio University, Osaka University, and the National Institute for Basic Biology, including the Program for the Advancement of Research in Core Projects on Longevity of the Keio University Global Research Institute (H.O.). This study was also supported by the Office of the Assistant Secretary of Defense for Health Affairs through the Peer Reviewed Medical Research Program under Award W81XWH2010199 (N.I.), and by Award 1U54HD090257-01 from the NIH, and the District of Columbia Intellectual and Developmental Disabilities Research Center Award program.

1. P. Grandjean, P. J. Landrigan, Developmental neurotoxicity of industrial chemicals. *Lancet* **368**, 2167–2178 (2006).
2. B. L. Thompson, P. Levitt, G. D. Stanwood, Prenatal exposure to drugs: Effects on brain development and implications for policy and education. *Nat. Rev. Neurosci.* **10**, 303–312 (2009).
3. P. A. May *et al*., Prevalence of fetal alcohol spectrum disorders in 4 US communities. *JAMA* **319**, 474–482 (2018).
4. Y. Tang, R. Liu, P. Zhao, Ketamine: An update for obstetric anesthesia. *Transl. Perioper. Pain Med.* **4**, 1–12 (2017).
5. C. Ikonomidou, Triggers of apoptosis in the immature brain. *Brain Dev.* **31**, 488–492 (2009).
6. S. Kirischuk *et al*., Modulation of neocortical development by early neuronal activity: Physiology and pathophysiology. *Front. Cell. Neurosci.* **11**, 379 (2017).
7. B. D. Semple, K. Blomgren, K. Gimlin, D. M. Ferriero, L. J. Noble-Haeusslein, Brain development in rodents and humans: Identifying benchmarks of maturation and vulnerability to injury across species. *Prog. Neurobiol.* **106-107**, 1–16 (2013).
8. J. R. Wozniak, A. Y. Klintsova, D. A. Hamilton, S. M. Mooney, Proceedings of the 2017 annual meeting of the Fetal Alcohol Spectrum Disorders study group. *Alcohol* **69**, 7–14 (2018).
9. C. Holzman, N. Paneth, R. Little, J. Pinto-Martin; Neonatal Brain Hemorrhage Study Team, Perinatal brain injury in premature infants born to mothers using alcohol in pregnancy. *Pediatrics* **95**, 66–73 (1995).
10. S. M. Mooney, E. I. Varlinskaya, Acute prenatal exposure to ethanol and social behavior: Effects of age, sex, and timing of exposure. *Behav. Brain Res.* **216**, 358–364 (2011).
11. M. L. Schneider, C. F. Moore, G. W. Kraemer, Moderate alcohol during pregnancy: Learning and behavior in adolescent rhesus monkeys. *Alcohol. Clin. Exp. Res.* **25**, 1383–1392 (2001).
12. X. Wang *et al*., In utero MRI identifies consequences of early-gestation alcohol drinking on fetal brain development in rhesus macaques. *Proc. Natl. Acad. Sci. U.S.A.* **117**, 10035–10044 (2020).
13. D. F. Wozniak *et al*., Apoptotic neurodegeneration induced by ethanol in neonatal mice is associated with profound learning/memory deficits in juveniles followed by progressive functional recovery in adults. *Neurobiol. Dis.* **17**, 403–414 (2004).
14. C. Ikonomidou *et al*., Ethanol-induced apoptotic neurodegeneration and fetal alcohol syndrome. *Science* **287**, 1056–1060 (2000).
15. J. H. Krystal, C. G. Abdallah, G. Sanacora, D. S. Charney, R. S. Duman, Ketamine: A paradigm shift for depression research and treatment. *Neuron* **101**, 774–778 (2019).
16. R. N. Moda-Sava *et al*., Sustained rescue of prefrontal circuit dysfunction by antidepressant-induced spine formation. *Science* **364**, eaat8078 (2019).
17. O. Corazza, S. Assi, F. Schifano, From "special K" to "special M": The evolution of the recreational use of ketamine and methoxetamine. *CNS Neurosci. Ther.* **19**, 454–460 (2013).

18. H. M. Cheung, D. T. W. Yew, Effects of perinatal exposure to ketamine on the developing brain. *Front. Neurosci.* **13**, 138 (2019).
19. S. Chomchai, J. Phuditshinnapatra, P. Mekavuthikul, C. Chomchai, Effects of unconventional recreational drug use in pregnancy. *Semin. Fetal Neonatal Med.* **24**, 142–148 (2019).
20. M. G. Paule *et al*., Ketamine anesthesia during the first week of life can cause long-lasting cognitive deficits in rhesus monkeys. *Neurotoxicol. Teratol.* **33**, 220–230 (2011).
21. L. Huang, Y. Liu, W. Jin, X. Ji, Z. Dong, Ketamine potentiates hippocampal neurodegeneration and persistent learning and memory impairment through the PKCγ-ERK signaling pathway in the developing brain. *Brain Res.* **1476**, 164–171 (2012).
22. R. T. Wilder *et al*., Early exposure to anesthesia and learning disabilities in a population-based birth cohort. *Anesthesiology* **110**, 796–804 (2009).
23. K. Kagias, C. Nehammer, R. Pocock, Neuronal responses to physiological stress. *Front. Genet.* **3**, 222 (2012).
24. S. Ishii, K. Hashimoto-Torii, Impact of prenatal environmental stress on cortical development. *Front. Cell. Neurosci.* **9**, 207 (2015).
25. M. Pietrucha-Dutczak, M. Amadio, S. Govoni, J. Lewin-Kowalik, A. Smedowski, The role of endogenous neuroprotective mechanisms in the prevention of retinal ganglion cells degeneration. *Front. Neurosci.* **12**, 834 (2018).
26. E. C. Oh, N. Katsanis, Cilia in vertebrate development and disease. *Development* **139**, 443–448 (2012).
27. J. I. Arellano, S. M. Guadiana, J. J. Breunig, P. Rakic, M. R. Sarkisian, Development and distribution of neuronal cilia in mouse neocortex. *J. Comp. Neurol.* **520**, 848–873 (2012).
28. A. Guemez-Gamboa, N. G. Coufal, J. G. Gleeson, Primary cilia in the developing and mature brain. *Neuron* **82**, 511–521 (2014).
29. V. Singla, J. F. Reiter, The primary cilium as the cell's antenna: Signaling at a sensory organelle. *Science* **313**, 629–633 (2006).
30. J. Kim *et al*., Functional genomic screen for modulators of ciliogenesis and cilium length. *Nature* **464**, 1048–1051 (2010).
31. A. Marley, M. von Zastrow, DISC1 regulates primary cilia that display specific dopamine receptors. *PLoS One* **5**, e10902 (2010).
32. A. Marley, M. von Zastrow, A simple cell-based assay reveals that diverse neuropsychiatric risk genes converge on primary cilia. *PLoS One* **7**, e46647 (2012).
33. J. L. Nanson, Autism in fetal alcohol syndrome: A report of six cases. *Alcohol. Clin. Exp. Res.* **16**, 558–565 (1992).
34. S. L. Fryer, C. L. McGee, G. E. Matt, E. P. Riley, S. N. Mattson, Evaluation of psychopathological conditions in children with heavy prenatal alcohol exposure. *Pediatrics* **119**, e733–e741 (2007).
35. C. M. Coronel-Oliveros, R. Pacheco-Calderón, Prenatal exposure to ketamine in rats: Implications on animal models of schizophrenia. *Dev. Psychobiol.* **60**, 30–42 (2018).
36. C. J. Haycraft *et al*., Intraflagellar transport is essential for endochondral bone formation. *Development* **134**, 307–316 (2007).
37. J. A. Gorski *et al*., Cortical excitatory neurons and glia, but not GABAergic neurons, are produced in the Emx1-expressing lineage. *J. Neurosci.* **22**, 6309–6314 (2002).
38. N. F. Berbari *et al*., Hippocampal and cortical primary cilia are required for aversive memory in mice. *PLoS One* **9**, e106576 (2014).
39. J. Snedeker *et al*., Unique spatiotemporal requirements for intraflagellar transport genes during forebrain development. *PLoS One* **12**, e0173258 (2017).
40. J. W. Olney *et al*., Ethanol-induced caspase-3 activation in the in vivo developing mouse brain. *Neurobiol. Dis.* **9**, 205–219 (2002).
41. A. P. Ghosh *et al*., The proapoptotic BH3-only, Bcl-2 family member, Puma is critical for acute ethanol-induced neuronal apoptosis. *J. Neuropathol. Exp. Neurol.* **68**, 747–756 (2009).
42. D. Goldowitz *et al*., Molecular pathways underpinning ethanol-induced neurodegeneration. *Front. Genet.* **5**, 203 (2014).
43. B. T. Hyman, J. Yuan, Apoptotic and non-apoptotic roles of caspases in neuronal physiology and pathophysiology. *Nat. Rev. Neurosci.* **13**, 395–406 (2012).
44. D. J. Simon *et al*., A caspase cascade regulating developmental axon degeneration. *J. Neurosci.* **32**, 17540–17553 (2012).
45. J. D. Sokolowski *et al*., Caspase-mediated cleavage of actin and tubulin is a common feature and sensitive marker of axonal degeneration in neural development and injury. *Acta Neuropathol. Commun.* **2**, 16 (2014).
46. M. L. Hendrickson, C. Ling, R. E. Kalil, Degeneration of axotomized projection neurons in the rat dLGN: Temporal progression of events and their mitigation by a single administration of FGF2. *PLoS One* **7**, e46918 (2012).
47. D. Davalos *et al*., ATP mediates rapid microglial response to local brain injury in vivo. *Nat. Neurosci.* **8**, 752–758 (2005).
48. A. Nimmerjahn, F. Kirchhoff, F. Helmchen, Resting microglial cells are highly dynamic surveillants of brain parenchyma in vivo. *Science* **308**, 1314–1318 (2005).
49. G. A. Bishop, N. F. Berbari, J. Lewis, K. Mykytyn, Type III adenylyl cyclase localizes to primary cilia throughout the adult mouse brain. *J. Comp. Neurol.* **505**, 562–571 (2007).
50. N. Delcourt *et al*., PACAP type I receptor transactivation is essential for IGF-1 receptor signalling and antiapoptotic activity in neurons. *EMBO J.* **26**, 1542–1551 (2007).
51. C. A. Bondy, W. H. Lee, Patterns of insulin-like growth factor and IGF receptor gene expression in the brain. Functional implications. *Ann. N. Y. Acad. Sci.* **692**, 33–43 (1993).
52. D. Zhu, S. Shi, H. Wang, K. Liao, Growth arrest induces primary-cilium formation and sensitizes IGF-1-receptor signaling during differentiation induction of 3T3-L1 preadipocytes. *J. Cell Sci.* **122**, 2760–2768 (2009).
53. C. Yeh *et al*., IGF-1 activates a cilium-localized noncanonical Gβγ signaling pathway that regulates cell-cycle progression. *Dev. Cell* **26**, 358–368 (2013).
54. H. Jo *et al*., Small molecule-induced cytosolic activation of protein kinase Akt rescues ischemia-elicited neuronal death. *Proc. Natl. Acad. Sci. U.S.A.* **109**, 10581–10586 (2012).
55. B. D. Manning, L. C. Cantley, AKT/PKB signaling: Navigating downstream. *Cell* **129**, 1261–1274 (2007).
56. A. Brunet, S. R. Datta, M. E. Greenberg, Transcription-dependent and -independent control of neuronal survival by the PI3K-Akt signaling pathway. *Curr. Opin. Neurobiol.* **11**, 297–305 (2001).
57. S. M. Guadiana *et al*., Arborization of dendrites by developing neocortical neurons is dependent on primary cilia and type 3 adenylyl cyclase. *J. Neurosci.* **33**, 2626–2638 (2013).
58. N. Spassky *et al*., Primary cilia are required for cerebellar development and Shh-dependent expansion of progenitor pool. *Dev. Biol.* **317**, 246–259 (2008).
59. G. J. Pazour *et al*., Chlamydomonas IFT88 and its mouse homologue, polycystic kidney disease gene tg737, are required for assembly of cilia and flagella. *J. Cell Biol.* **151**, 709–718 (2000).
60. B. Halliwell, Oxidative stress in cell culture: An under-appreciated problem? *FEBS Lett.* **540**, 3–6 (2003).
61. A. J. Canty, M. Murphy, Molecular mechanisms of axon guidance in the developing corticospinal tract. *Prog. Neurobiol.* **85**, 214–235 (2008).
62. M. Ueno *et al*., Layer V cortical neurons require microglial support for survival during postnatal development. *Nat. Neurosci.* **16**, 543–551 (2013).
63. J. W. Olney *et al*., Ethanol-induced apoptotic neurodegeneration in the developing C57BL/6 mouse brain. *Brain Res. Dev. Brain Res.* **133**, 115–126 (2002).
64. W. Slikker Jr., *et al*., Ketamine-induced neuronal cell death in the perinatal rhesus monkey. *Toxicol. Sci.* **98**, 145–158 (2007).
65. A. M. Brambrink *et al*., Ketamine-induced neuroapoptosis in the fetal and neonatal rhesus macaque brain. *Anesthesiology* **116**, 372–384 (2012).
66. A. Florentin, E. Arama, Caspase levels and execution efficiencies determine the apoptotic potential of the cell. *J. Cell Biol.* **196**, 513–527 (2012).
67. E. Kuranaga, M. Miura, Nonapoptotic functions of caspases: Caspases as regulatory molecules for immunity and cell-fate determination. *Trends Cell Biol.* **17**, 135–144 (2007).
68. C. L. Cusack, V. Swahari, W. Hampton Henley, J. Michael Ramsey, M. Deshmukh, Distinct pathways mediate axon degeneration during apoptosis and axon-specific pruning. *Nat. Commun.* **4**, 1876 (2013).
69. A. Ertürk, Y. Wang, M. Sheng, Local pruning of dendrites and spines by caspase-3-dependent and proteasome-limited mechanisms. *J. Neurosci.* **34**, 1672–1688 (2014).
70. A. Nikolaev, T. McLaughlin, D. D. O'Leary, M. Tessier-Lavigne, APP binds DR6 to trigger axon pruning and neuron death via distinct caspases. *Nature* **457**, 981–989 (2009).
71. S. Subbanna *et al*., G9a-mediated histone methylation regulates ethanol-induced neurodegeneration in the neonatal mouse brain. *Neurobiol. Dis.* **54**, 475–485 (2013).
72. G. D. Gale *et al*., A genome-wide panel of congenic mice reveals widespread epistasis of behavior quantitative trait loci. *Mol. Psychiatry* **14**, 631–645 (2009).
73. T. M. Keane *et al*., Mouse genomic variation and its effect on phenotypes and gene regulation. *Nature* **477**, 289–294 (2011).
74. M. Loos *et al*.; Neuro-BSIK Mouse Phenomics Consortium, Within-strain variation in behavior differs consistently between common inbred strains of mice. *Mamm. Genome* **26**, 348–354 (2015).
75. S. M. de la Monte, X. J. Xu, J. R. Wands, Ethanol inhibits insulin expression and actions in the developing brain. *Cell. Mol. Life Sci.* **62**, 1131–1145 (2005).
76. F. X. Zhang, R. Rubin, T. A. Rooney, Ethanol induces apoptosis in cerebellar granule neurons by inhibiting insulin-like growth factor 1 signaling. *J. Neurochem.* **71**, 196–204 (1998).
77. L. He *et al*., Dose-dependent effects of alcohol on insulin signaling: Partial explanation for biphasic alcohol impact on human health. *Mol. Endocrinol.* **21**, 2541–2550 (2007).
78. J. W. Ting, W. W. Lautt, The effect of acute, chronic, and prenatal ethanol exposure on insulin sensitivity. *Pharmacol. Ther.* **111**, 346–373 (2006).
79. M. Dean *et al*., Acute ethanol increases IGF-I-induced phosphorylation of ERKs by enhancing recruitment of p52-Shc to the Grb2/Shc complex. *J. Cell. Physiol.* **232**, 1275–1286 (2017).
80. M. K. Lehtinen *et al*., The cerebrospinal fluid provides a proliferative niche for neural progenitor cells. *Neuron* **69**, 893–905 (2011).
81. Y. Nishimura, K. Kasahara, T. Shiromizu, M. Watanabe, M. Inagaki, Primary cilia as signaling hubs in health and disease. *Adv. Sci. (Weinh.)* **6**, 1801138 (2018).
82. J. Andrae, R. Gallini, C. Betsholtz, Role of platelet-derived growth factors in physiology and medicine. *Genes Dev.* **22**, 1276–1312 (2008).
83. E. M. Toledo, M. Colombres, N. C. Inestrosa, Wnt signaling in neuroprotection and stem cell differentiation. *Prog. Neurobiol.* **86**, 281–296 (2008).

84. N. Miao *et al*., Sonic hedgehog promotes the survival of specific CNS neuron populations and protects these cells from toxic insult in vitro. *J. Neurosci.* **17**, 5891–5899 (1997).
85. K. Yoshimura, T. Kawate, S. Takeda, Signaling through the primary cilium affects glial cell survival under a stressed environment. *Glia* **59**, 333–344 (2011).
86. D. Kopinke, E. C. Roberson, J. F. Reiter, Ciliary hedgehog signaling restricts injury-induced adipogenesis. *Cell* **170**, 340–351.e12 (2017).
87. V. Dubreuil, A. M. Marzesco, D. Corbeil, W. B. Huttner, M. Wilsch-Bräuninger, Midbody and primary cilium of neural progenitors release extracellular membrane particles enriched in the stem cell marker prominin-1. *J. Cell Biol.* **176**, 483–495 (2007).
88. G. Garcia 3rd, D. R. Raleigh, J. F. Reiter, How the ciliary membrane is organized inside-out to Communicate outside-in. *Curr. Biol.* **28**, R421–R434 (2018).
89. S. C. Phua *et al*., Dynamic remodeling of membrane composition drives cell cycle through primary cilia excision. *Cell* **168**, 264–279.e15 (2017).
90. G. Novarino, N. Akizu, J. G. Gleeson, Modeling human disease in humans: The ciliopathies. *Cell* **147**, 70–79 (2011).
91. M. Pruski, B. Lang, Primary cilia-an underexplored topic in major mental illness. *Front. Psychiatry* **10**, 104 (2019).
92. S. Ishii *et al*., Variations in brain defects result from cellular mosaicism in the activation of heat shock signalling. *Nat. Commun.* **8**, 15157 (2017).
93. S. Mohammad *et al*., Kcnn2 blockade reverses learning deficits in a mouse model of fetal alcohol spectrum disorders. *Nat. Neurosci.* **23**, 533–543 (2020).
94. A. E. Ayoub, A. K. Salm, Increased morphological diversity of microglia in the activated hypothalamic supraoptic nucleus. *J. Neurosci.* **23**, 7759–7766 (2003).
95. F. Verdonk *et al*., Phenotypic clustering: A novel method for microglial morphology analysis. *J. Neuroinflammation* **13**, 153 (2016).
96. R. Kongsui, S. B. Beynon, S. J. Johnson, F. R. Walker, Quantitative assessment of microglial morphology and density reveals remarkable consistency in the distribution and morphology of cells within the healthy prefrontal cortex of the rat. *J. Neuroinflammation* **11**, 182 (2014).